# Bio-based formulation of an electrically conductive ink with high potential for additive manufacturing by direct ink writing

Khaoula Bouzidi, Didier Chaussy, Alessandro Gandini, Emmanuel Flahaut, Roberta Bongiovanni, Davide Beneventi

# Bio-based formulation of an electrically conductive ink with high potential for additive manufacturing by direct ink writing

**Khaoula Bouzidi [a,*], Didier Chaussy [a], Alessandro Gandini, Emmanuel Flahaut [b], Roberta Bongiovanni [c], Davide Beneventi [a]**

[a] Univ. Grenoble Alpes, CNRS, Grenoble INP[+], LGP2, 38000 Grenoble, France

[+] Institute of engineering Univ. Grenoble Alpes

[b] CIRIMAT, Universite de Toulouse, CNRS, INPT, UPS, UMR CNRS-UPS-INP 5085, Université de Toulouse 3 Paul Sabatier, Bat. CIRIMAT, 118, route de Narbonne, 31062, Toulouse cedex 9, France

[c] Department of Applied Science and Technology, Politecnico di Torino, Torino, 10129 Italy

**Abstract**

In this work, a new ink formulation based on the use of a fully bio-based thermosetting resin as a binder, cellulose powders as rheology modifiers, and carbon nanotubes as conductive fillers was developed, and its potential as a functional material for additive manufacturing by direct ink writing was demonstrated. Electrical and rheological characterization of the nanocomposite at increasing CNT and cellulose concentrations was conducted in order to determine the optimal processing conditions and the printability window for the system. In addition, the resulting nanocomposite was further carbonized to yield a carbon-carbon nanocomposite with a better electrical conductivity. The results of the present study open the possibility of either integrating conductive circuits in a 3D-printed structure, or the

[*] Corresponding author.

Email address: Khaoula.bouzidi@grenoble-inp.fr

printing of a bulk semi-conductive complex structure using a low-cost DIW 3D printing technique and mostly cost-effective renewable raw materials.

**Keywords:** Carbon nanotubes; Rheology; Electrical properties; Biocomposites; 3D printing

## 1 Introduction

Additive manufacturing, also referred to as 3D printing or additive fabrication, is a revolutionary manufacturing technology arising significant interest in recent years. It is indeed revolutionary and also evolutionary, leading manufacturers to reconceptualize the approach used to develop, produce and design objects. Due to its adaptability and controllable parameters, a myriad of applications are possible. In addition, at a time when environmental concerns are increasing, this process uses limited consumables, offers customizable object geometry using the same machines, and is also cost-effective That is why this technology is being used to manufacture different objects in many fields. One of the most trendy topics is the development of functional materials, and particularly electrically conductive materials which can be used in many applications such as energy storage and sensors [1]. In the literature, one can find the use of different 3D printing techniques to obtain electrically conductive printed objects such as the addition of electrically conductive fillers in thermoplastics yielding conductive filaments [2,3] which can then be used in 3D printing by filament fused fabrication (FFF), or the addition of these fillers in UV curable resins using the SLA technique [4]. However, the conductivity of these materials remains limited because of the low filler content that can be blended into such polymers. Accordingly, most research work has focused on the development of highly conductive inks for 3D printing by direct ink extrusion, which consists of extruding and depositing pasty ink materials through a nozzle at ambient temperature without material

phase transition for supporting the printed structure. This printing technique allows the proper tailoring of the composite material paving the way to the use of many non-melting binders and fillers such as cellulose fibers, hydrogels, and thermosetting resins [5–7].
In the literature, various printable conductive inks were developed for 3D printing by direct ink writing (DIW) by adding conductive particles such as graphene, silver wires, carbon black, and carbon nanotubes (CNTs) [6,8–12] to different kinds of oligomers and polymers such as epoxy resin precursors [6], PLA solution [9], acrylate monomers [11], and poly(ethylene oxide) [13].

In order to successfully develop such conductive printable inks, the formulation should fulfill the printability requirements characterized by (i) an extrudable homogeneous filament without nozzle clogging, (ii) shape maintenance of the extruded filament, and (iii) shape fidelity after solidification [14]. Moreover, the extruded filaments, which form the building block of future printed objects or circuits, should also conduct as many electrons as possible after solidification. The use of carbon nanotubes as conductive fillers in conductive inks is well-known thanks to their low percolation threshold leading to conductive polymeric composite. CNT-based composites are already studied and investigated yielding good electrical conductive films and organic capacitors and sensors [15]. However, one of the challenges of the use of such fillers is their high aspect ratio and strong steric interactions which cause entanglement of CNTs and the formation of agglomerates which can limit the ink printability because of nozzle clogging [16,17]. Hence, the morphological choice of the used CNTs and the quality of the dispersion has to be first assessed to optimize both the printability and the electrical conductivity of the developed ink. The binder choice is also very important since it must be compatible with the filler and act as a good dispersing medium of the nanoparticles. Thermosetting resins are such an example thanks to the

possibility to tailor their viscosity and their good affinity with CNTs [18–20]. Moreover, when using organic polymers, the matrix phase can be further carbonized to increase the overall electrical conductivity of the nanocomposite. Indeed, organic polymers with high carbon and limited oxygen content can usually be carbonized and, in the case of some polymers, even graphitized. Furan resins, and in particular polyfurfuryl alcohol, fulfill these carbonization requirements with a char residue reaching up to 50 wt%. Thus, this polymer is largely used as a precursor for a non-graphitizing carbon called glassy carbon resulting in a lower electrical conductivity compared to graphite, but with an improved hardness [21–23]. A study of the Raman spectra of PFA pyrolyzed at different temperatures revealed some critical temperatures. At 400°C carbonization starts, at 550°C graphite nucleation appears, at 700°C crystallite growth is observed, and above that temperature, crystallite size increases [24].

Accordingly, in the present work, we have investigated the possibility to formulate a new conductive 'ink' for additive manufacturing using for the first time a bio-based furanic resin coupled with carbon nanotubes and cellulosic fillers. To do so, we started with a study on the effect of CNTs morphology on both the dispersion ability in ethanol and the rheology. Later, different formulations were prepared to optimize the rheological behavior, hence their printability potential, as well as their electrical conductivity. Finally, a pyrolysis step was conducted to assess the eventual increase in electrical conductivity.

## 2 Material and methods

### 2.1 Materials

A commercial poly(furfuryl alcohol) (PFA) resin and a latent catalyst were kindly supplied by Transfurans Chemicals (Belgium). The commercial resin contains 7.5 wt% water and less than 1% of free monomer. The cellulosic fillers was a commercial cellulose powder kindly supplied

by the Rossow Industry. The measured water content of these particles was 4.58 ±0.05 wt%. As determined using granulometric analysis, 50% of the particles have a size under 9.8 µm. Moreover, as one can see in the SEM image (Fig. 1), these cellulosic particles have a small aspect ratio.

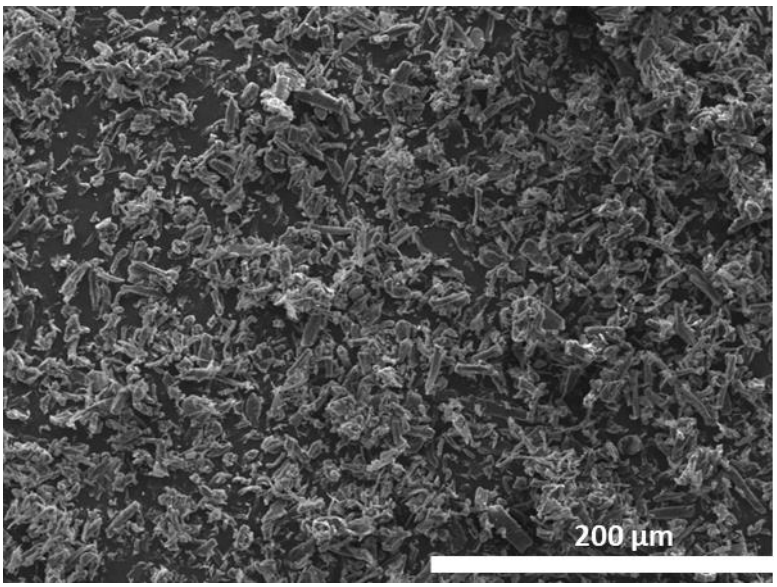


*Fig. 1. SEM image of the used cellulose powder.*

In this work, CNTs were selected as functional fillers because they (i) confer a shear-thinning flow behavior and their shape stability compatible with the requirements of 3D printing by extrusion, (ii) can be aligned by the shear applied in the nozzle, thus improving the electrical conductivity, and (iii) have a low percolation threshold in PFA/cellulose composites [6,25]. Accordingly, commercial CNTs were purchased from *Nanoamor.* Different types and morphologies of CNT were used in order to select the most suitable one. Their main characteristics, given by the supplier, are listed in Table 1. The aspect ratio, defined as the ratio between the length and diameter, ranged from 33 to 2500 and their bulk electrical conductivity (EC) was ca. 100 S/cm (supplier data). The EC was experimentally measured by

the 4 probes technique on a thin layer of CNT (ca. 12 µm) on a glass substrate and was found to be in line with the supplier's indications.

*Table 1. The commercial CNT characteristics.*

| Labeled | Supplier's reference | Internal diameter (nm) | External diameter (nm) | Length (nm) | Aspect ratio L/d | EC (S/cm) |
|---|---|---|---|---|---|---|
| **SWCNT** | 1283YJ | | 1-2 | 5000-30000 | 2500 | >100 |
| **DWCNT** | 1280YJD | 1-3 | 2-4 | 50000 | 1250-2500 | >100 |
| **MWCNT 1** | 1229YJ | 5-10 | 20-30 | 10000-30000 | 333-1500 | >100 |
| **MWCNT 2** | 1233YJ | 5-15 | 30-80 | <10000 | 125-333 | >100 |
| **MWCNT Gr** | 1223YJ | 5-15 | 30-80 | <10000 | 125-333 | >100 |
| **MWCNT short** | 1235YJS | 3-5 | 8-15 | 500-2000 | 33-250 | >100 |

2.2 Methods

The commercial CNTs described in Table 1 were received in powder form, hence a suspension preparation step was needed. In this work, we chose to prepare the suspension using ethanol as liquid carrier for optimal dilution of the PFA resin and easy solvent evaporation. Suspensions of 1 wt% of the different CNTs in ethanol were prepared by hand stirring with the added dispersant agent provided by the supplier which is a mixture of nonionic surfactants in polymerized form (*Nanoamor 8011YJ, USA*). The dispersant was added at different concentrations following the supplier's recommendations depending on

the used CNT type and morphology. The dispersion of these nanoparticles was carried out at first with sonication. This ultrasonic treatment was applied by introducing a titanium-based probe powered by a *Branson 250* bath ultrasounds generator with a power of 200 W at 20 kHz. All the suspensions were sonicated in a discontinuous mode for 30 min with 10 min intervals to avoid overheating. Moreover, the suspensions were covered and placed in an ice bath to limit solvent evaporation. Afterward, the CNT suspensions were further homogenized using an ultra-turrax (Unidrive x1000D) for 5 min at 10,000 rpm. The speed and duration were limited to prevent CNT breakage. The ensuing 1 wt% CNT suspensions were then stored for further use in sealed bottles to prevent solvent evaporation.

To prepare printable inks with suitable electrical conductivity CNT-based ink formulations were prepared using the previously prepared CNT-ethanol suspensions. To do so, the PFA resin was added to CNTs and then hand mixed. The cellulose was gradually added while mixing using the ultra-turrax at 7000 rpm for 10 min. The mixture was then placed on a hot plate with continuous magnetic stirring. The hot plate temperature was fixed at 78°C to evaporate the solvent in excess.

For further optimization, different formulations using either DWCNT or MWCNT-short were prepared with different concentrations of conductive fillers and cellulose. These formulations allowed studying the effect of CNT morphology and concentration and cellulose addition on the ink rheology and electrical conductivity. The different formulations are detailed in Table 2.

*Table 2. Conductive formulations detailed weight ratios and fillers type.*

| CNT type | Formulation reference | PFA (wt%) | CNT content (wt%) | Cellulose (wt%) |
|---|---|---|---|---|
| DWCNT | DCNT-4-20 | 76.5 | 4.0 | 19.5 |
| MWCNT-Short | MCNT-4-20 | 76.5 | 4.0 | 19.5 |
| DWCNT | DCNT-4-15 | 81 | 4.0 | 15.0 |
| MWCNT-Short | MCNT-4-15 | 81.0 | 4.0 | 15.0 |
| DWCNT | DCNT-4 | 96.0 | 4.0 | 0.0 |
| MWCNT-Short | MCNT-4 | 96.0 | 4.0 | 0.0 |
| DWCNT | DCNT-1.5-20 | 79.0 | 1.5 | 19.5 |
| MWCNT-Short | MCNT-1.5-20 | 79.0 | 1.5 | 19.5 |
| DWCNT | DCNT-1.5 | 98.5 | 1.5 | 0 |
| MWCNT-Short | MCNT-1.5 | 98.5 | 1.5 | 0 |
| DWCNT | DCNT-0.5-20 | 80.0 | 0.5 | 19.5 |
| MWCNT-Short | MCNT-0.5-20 | 80.0 | 0.5 | 19.5 |
| DWCNT | DCNT-0.5 | 99.5 | 0.5 | 0.0 |
| MWCNT-Short | MCNT-0.5 | 99.5 | 0.5 | 0.0 |

After formulating inks, the resulting cured composites could be carbonized thanks to the use of poly(furfuryl alcohol) polymers which have a char residue of at least 50 wt% [26,27]. The pyrolysis step was performed to yield a carbon/carbon composite. The pyrolysis of cured

composites was performed in a tubular oven (*Carbolite®, type 3216*) under nitrogen flux until 950°C. The heating profile was slow and meticulous with a heating rate between 0.1 and 0.2 °C/min when exceeding 300°C in order to avoid any deformation or break caused by violent volatiles release.

To assess the rheological behavior of the CNT dispersions and the ink formulations, a parallel plate-plate measuring device of 25 mm in diameter was used on an *MCR 301* rheometer *(Anton Paar, Austria).* The gap between the plate and the platform was set to 1 mm and the temperature was fixed at 25°C. Before any rheological measurement, the fluids were sheared at a shear rate of 100 1/s for 200 seconds, followed by a rest of 200 seconds to reset any previous shear history and the samples were covered to avoid any solvent evaporation. To perform the flow curve experiments, the shear rate was increased from 0.1 to 100 1/s during which the viscosity was recorded. Oscillatory tests were also conducted to evaluate the viscoelastic properties of the prepared inks. Accordingly, amplitude sweep tests were performed at the frequency of 1 Hz and strain ranging from 0.001 to 100%. The evolution of the storage modulus (G') and loss modulus (G"), as a function of strain, or stress was analyzed.

The morphology of the composite cross-section in form of extruded filaments was investigated by scanning electron microscopy (SEM). The specimens were gold coated and examined using a *QuantaFEG250* instrument. The accelerating voltage was set at 2.50 kV and the magnification between X60 and X2000.

The conductivity of extruded and cured filaments was measured using an ohm-meter (*HP 34401A multimeter*). Hook-type probes were used for an optimized contact with the

filament. The electrical resistance between the two ends of the 2 to 5 cm long filament was then measured at least in triplicate. The Electrical Conductivity (EC), was calculated as:

$$EC = \frac{L}{R \cdot S} \qquad (1)$$

where L is the length between the two probes, R is the electrical resistance and S is the cross-section area of the filament.

To 3D print, we used a commercial Artillery sidewinder 3D printer. This commercial printer is compatible with thermoplastic filaments only, thus it was upgraded with a liquid deposition modeling (LDM) extruder (WASP Claystruder). The pasty formulation was fed to the LDM extruder and then driven by an Archimedes screw to the extrusion nozzle. In this work, we used a nozzle with a 0.72 mm diameter. The layer height, the road width, and the printing speed were fixed at respectively 0.45 mm, 0.72 mm, and 900 mm/min.

# 3 Results and discussions

## 3.1 Development and optimization of a printable electrically conductive ink

### 3.1.1 Suspension of CNTs in ethanol

According to the literature and the results of some preliminary tests, CNTs seem to have the highest potential for the formulation of a functional printable ink formulation. Nonetheless, one of the challenges that can be encountered is the high water content added to the formulation when increasing the fraction of CNTs. In the presence of PFA, water not only affects the rheological behavior of the formulation but also can lead to phase separation since PFA oligomers are miscible with a maximum 24 wt% of water. Moreover, the exothermal reaction of PFA oligomers can cause foaming and high porosity upon curing. To overcome these challenges, it was decided to disperse CNT powders in ethanol (a solvent of PFA resin that can be easily evaporated). Therefore, the choice of CNT type should be made

according to their dispersibility. Thereafter, 6 stock dispersions of 6 different CNT types (whose properties are given in Table 1) with different aspect ratios were prepared and their contents are detailed in Table 3.

*Table 3. Summary of components mass and weight fractions in the prepared CNT dispersions.*

| Reference | CNT (g) | Dispersant (g) (*Nanoamor*) | Ethanol (g) | Dispersant fraction | CNT (wt%) |
|---|---|---|---|---|---|
| **SWCNT** | 2.0 | 10.0 | 188 | 05:01 | 1.0 |
| **DWCNT** | 2.0 | 4.0 | 188 | 02:01 | 1.0 |
| **MWCNT 1** | 2.0 | 1.5 | 188 | 0.75:01 | 1.0 |
| **MWCNT 2** | 2.0 | 1.0 | 188 | 0.50:01 | 1.0 |
| **MWCNT Gr** | 2.0 | 1.0 | 188 | 0.50:01 | 1.0 |
| **MWCNT short** | 2.0 | 2.0 | 188 | 01:01 | 1.0 |

**Microscopic assessment of CNT dispersion**

As a first assessment, the stability of these dispersions was visually evaluated. As one can see in Fig. 2, after a few hours, most of the suspensions are visibly stable with no clear sedimentation except for SWCNT, where one can start noticing signs of sedimentation despite the important amount of added dispersant.

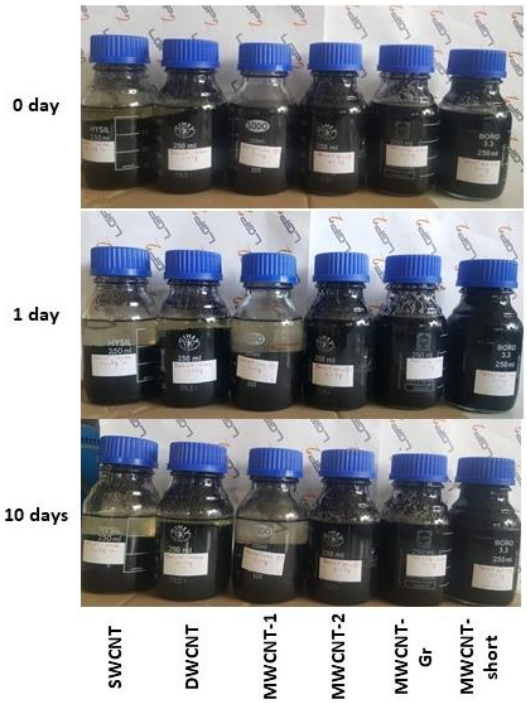


*Fig. 2. photographs of CNT dispersions after sonication and mechanical shearing.*

After 24 hours, the sedimentation of SWCNT started to be more noticeable and the same phenomenon was detected for MWCNT1 and DWCNT (these 3 CNT types have a high aspect ratio of 1500-2500). After 10 days, the same dispersion behavior was observed for the high aspect ratio CNT, whilst the suspensions with low aspect ratio CNT (<333) displayed a stable dispersion.

To further assess the homogeneity of the CNT suspensions, the 1 wt% CNT suspensions were then mixed with the PFA resin, which resulted in an overall 0.3 wt% concentration of CNTs. The suspensions were placed on glass supports to form a film to be observed with an optical microscope (white light). These observations are shown in Fig. 3.

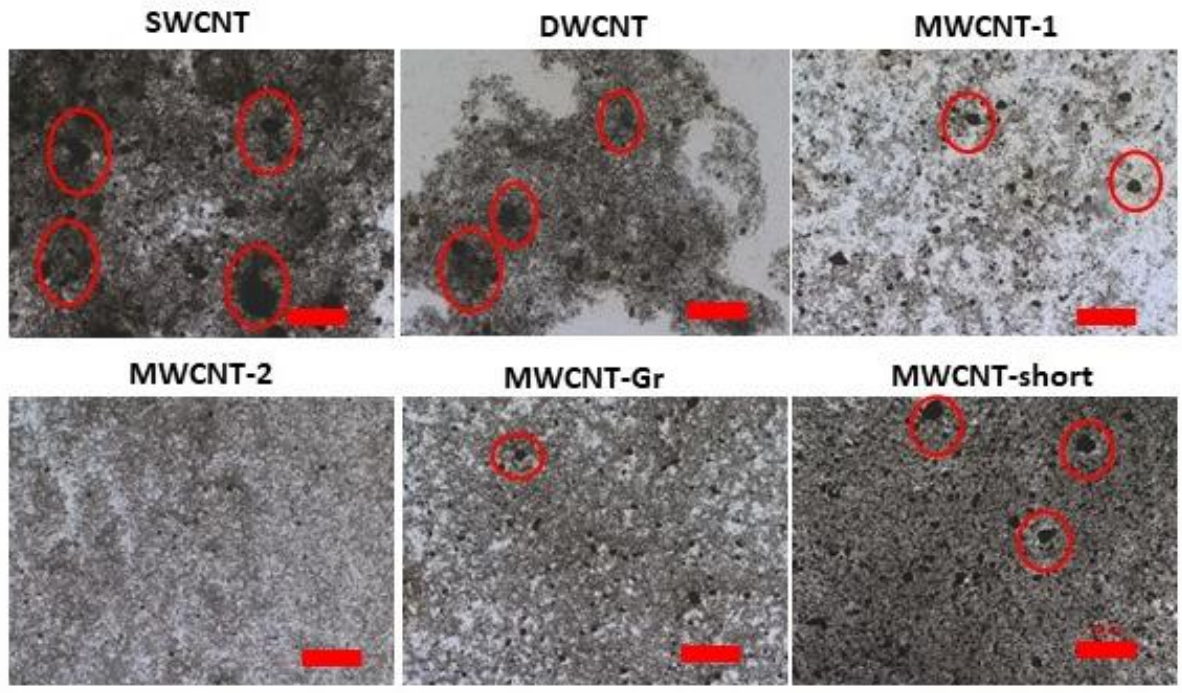


*Fig. 3. Optical microscopy images of 0.3 wt% CNT films in diluted PFA resin under the same magnification. Scale bar: 100 µm*

One can notice that the dispersion of SWCNT and DWCNT is not uniform and inhomogeneous with the presence of important aggregates and bundles, which is a classical issue when using high aspect ratio nanotubes [28]. The suspensions with an aspect ratio ranging from 33 (MWCNT-short) to 333 (MWCNT-2 and MWCNT-Gr) were easily dispersed despite the presence of some visible agglomerates. Despite the advantage of the use of a high aspect ratio of CNT to decrease the percolation threshold, these long CNTs have serious dispersion issues which can impair the electrical conductivity and the printability of the composite paste [29–31].

**Rheological assessment of CNT dispersion**

The flow behavior of the different suspensions in ethanol under a steady shear rate was studied. For each type of CNT, three suspensions with 1, 0.5, and 0.2 wt% concentrations were prepared and their flow curves are shown in Fig. 4-A, B, and C, respectively, where the

suspensions are named according to the CNT type and their concentration. By analyzing the flow curves, one can first notice a shear-thinning behavior which can be explained by the alignment of the CNTs in the shear direction and the disruption of the CNT network thus resulting in lower viscosity values. This shear-thinning behavior is proportional to the CNT concentration. Moreover, the viscosity evolution of the different CNT types as a function of their concentration measured at a shear rate of 0.1 1/s is summarized in Fig. 4-D. Similarly, the viscosity increases when increasing CNT concentration with a sharp increase when the concentration exceeds 0.5 wt%, thus suggesting a stronger entanglement. An exception should be made for the MWCNT-1 suspension which exhibited constant viscosity values. This can be explained by the poor dispersion (Fig. 3) and weak network interactions compared with those of the other suspensions. Furthermore, as one can notice in Fig. 4-C, at low CNT concentration (0.2 wt%) the flow is unstable with noticeable disruptions, especially for the SWCNT, which might be due to the important agglomeration and the non-uniform dispersion shown in Fig. 3. On the other hand, the suspensions that showed fewer agglomerates and a more uniform dispersion exhibited a more stable flow curve over the whole range of shearing rates. The flow of the suspension became more stable when increasing the CNT concentration, probably due to a stronger network interaction which decreases the influence of agglomerates. The short CNTs (MWCNT-short) and Long DWCNT exhibited the highest viscosity values for a concentration higher than 0.5 wt%, triggered in the first case by a good dispersion and in the second by the high aspect ratio.

Given the latter results, the short nanotubes (MWNCT-short) tended to have the best morphology in order to provide good and stable dispersions, resulting in a stable flow, higher viscosity, and a shear-thinning behavior needed for the future 3D printable ink. For the development of the printable formulation, different suspensions were prepared using

MWCNT-short and DWCNT with a concentration between 0.5 wt% (concentration from which a clear entanglement was noticed) and 4 wt%.

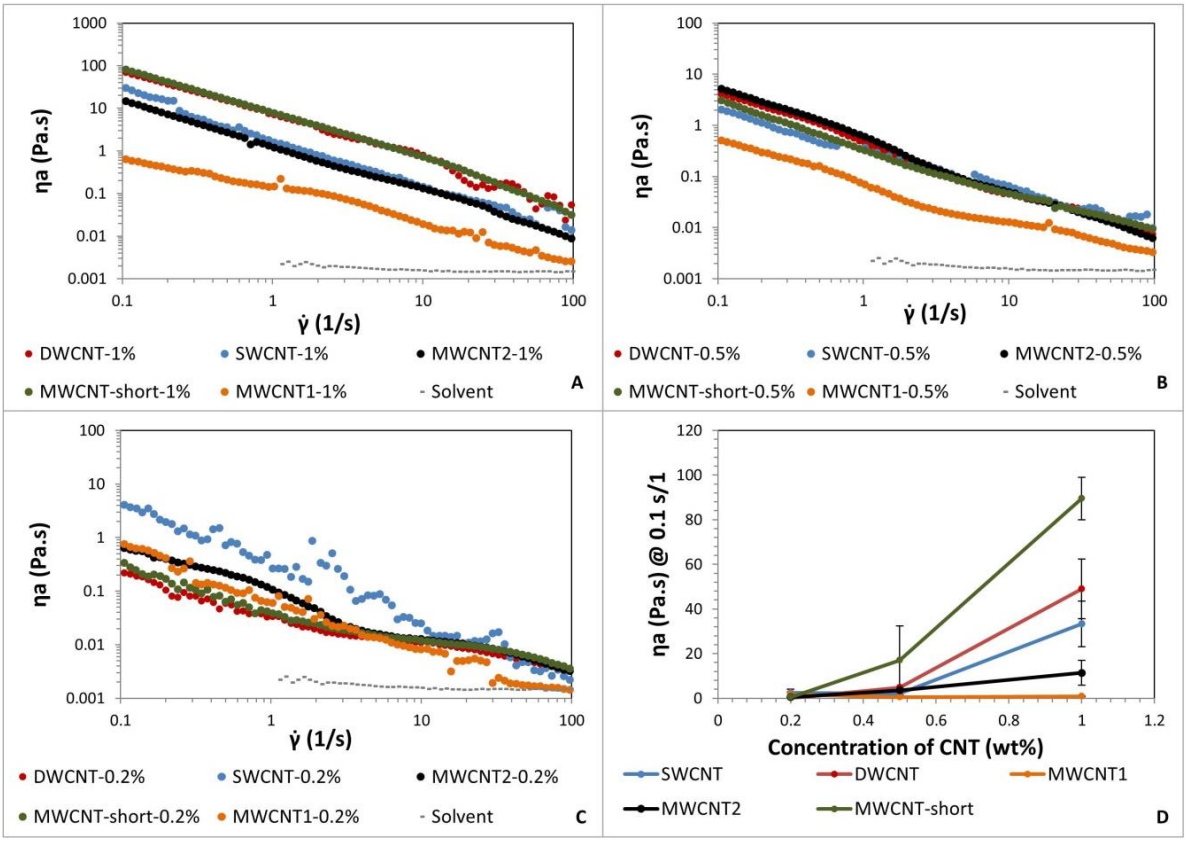


*Fig. 4. Viscosity and flow curves for CNT dispersions in ethanol at different concentrations.*

### 3.1.2 Conductive ink formulation

To obtain a conductive and 3D printable ink, different suspensions of DWCNT and MWCNT-short in PFA with and without cellulose powder were prepared. These suspensions are referred to as DCNT-x-y for the DWCNT and MCNT-x-y for MWCNT-short, with x being the CNT weight fraction and y the cellulose weight fraction in the formulation.

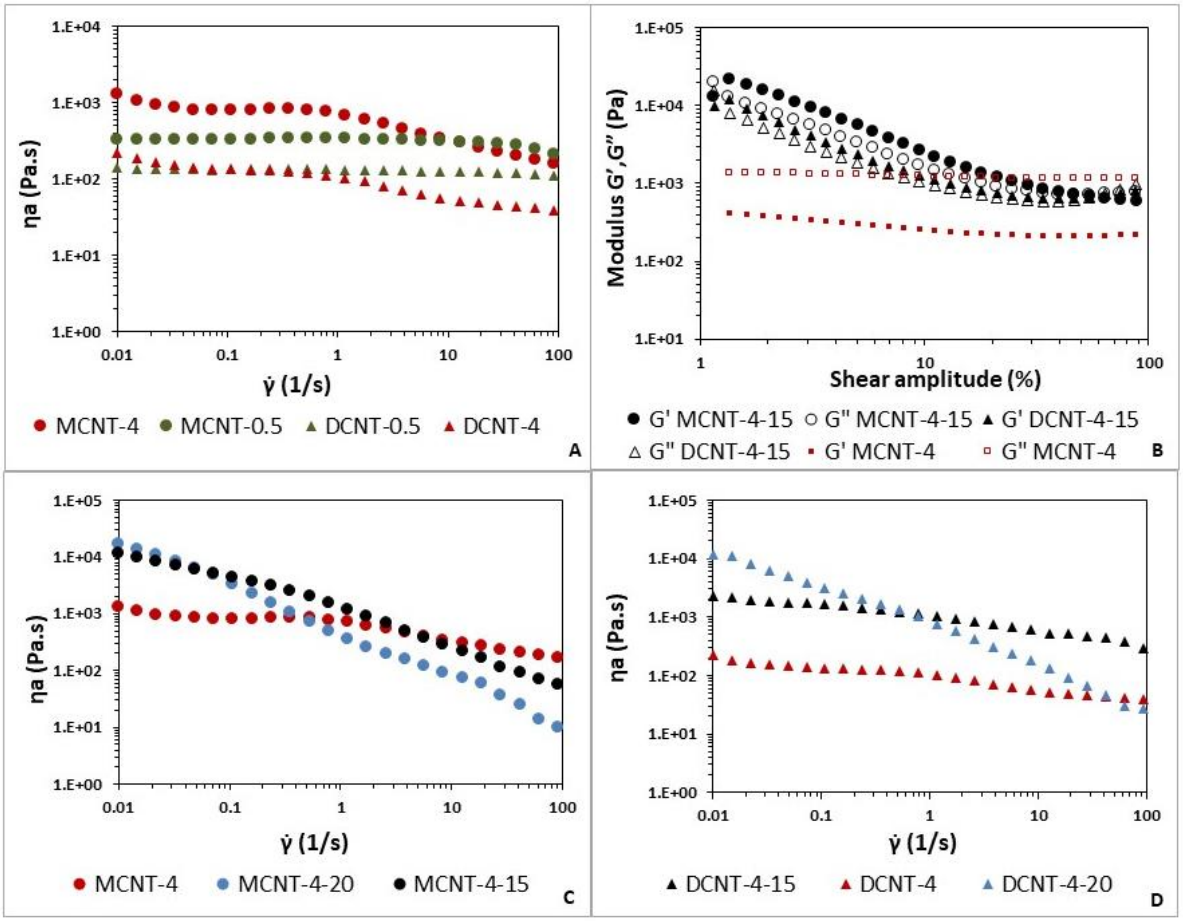


*Fig. 5. A), (B), and (C): Flow curves of conductive ink formulations and (D): amplitude sweep tests.*

Once again, a rheological characterization was necessary to assess the printability and thus determine the most adapted ink for 3D printing by cold material extrusion. To this end, the variation of the apparent viscosity with the shear rate of the 0.5 wt% and 4 wt% CNT dispersions was measured and shown in Fig. 5-A. A concentration of 0.5 wt% CNT in PFA results in a Newtonian flow behavior characterized by a constant viscosity. The viscosity of the suspension containing short MWCNT is higher than that with a high aspect ratio CNT, which correlates well with the results presented in the former section where the viscosities of the different stock suspensions were compared (Fig. 5-B). However, the shear-thinning behavior observed in the case of ethanol suspension was not detectable here, which is most

likely due to a poorer dispersion in the viscous PFA resin. When increasing the CNT content to 4 wt%, a shear-tinning behavior of the suspension started to appear with a clear increase in the apparent viscosity, especially for the formulation MCNT-4.

For a better assessment of the printability, an amplitude sweep test was carried out on the formulation. Fig. 5-B shows a dominance of the loss modulus over all the range of the shear amplitude negatively affecting the printability of the MCNT-4 dispersion. Therefore, more formulations were prepared with the addition of cellulose powder to tailor the rheology and enhance printability. The flow behavior of suspension containing 0, 15, and 20 wt% of cellulose at a constant CNT content (4 wt%) for both short and long nanotubes was analyzed and shown in Fig. 5-C/D. We can notice that in the case of low aspect ratio CNT, the addition of 15 wt% cellulose powder was enough to confer the suspension (MCNT-4-15) a pronounced highly shear-thinning behavior. On the other hand, when using high aspect ratio nanotubes, 15 wt% cellulose (DCNT-4-15) only increased the apparent viscosity of the suspension without any noticeable shear-thinning (in its flow). The addition of an extra 5 wt% cellulose (DCNT-4-20) was needed to form a stronger cellulose/CNT network to detect a shear-thinning flow triggered by the breakage of the network under shear stress. An amplitude sweep test of DCNT-4-15 and MCNT-4-15 was performed and the corresponding results are shown in Fig. 5-B. The storage modulus of the two formulations containing 15 wt% of cellulose is slightly higher than the loss modulus before a cross-over point corresponding to yield stresses of 770 ±170 Pa for MCNT-4-15 and 524 ±125 Pa for DCNT-4-15. However, the stiffness of both formulations cannot be easily assessed from these oscillatory rheology results, as G' starts to decrease in the tested strain range (from 1 to 100%). Nevertheless, the storage modulus of the formulation containing short nanotubes is higher, which can be explained by their better dispersion.

The addition of at least 15 wt% of cellulose is needed for yielding a shear-thinning flow necessary for a stable extrusion through the printing nozzle without clog formation. Moreover, the additional cellulose can increase the viscosity and the stiffness of the material in order to resist the printing force and also to obtain a viscoelastic material with high yield stress sufficient to bear the gravitational forces. The use of short nanotubes is also preferred because of their better dispersion.

To determine the effect of the addition of CNT to the PFA matrix, the volume electrical conductivity (EC) of CNT/PFA nanocomposites was evaluated from resistance measurements performed on nanocomposite filaments extruded from a 2 mm diameter nozzle with increasing CNT content (0.5–4 wt%).

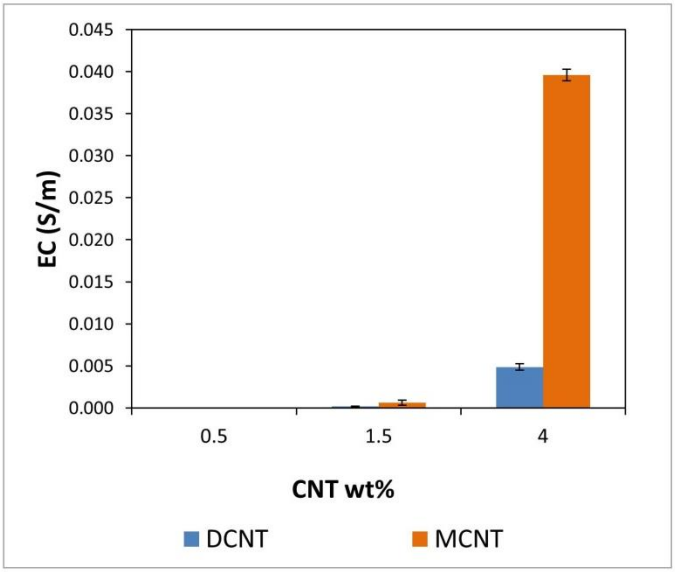


*Fig. 6. Electrical conductivity (EC) of extruded filaments of nanocomposite as a function CNT concentrations and type.*

As shown in Fig. 6, the resistivity of the nanocomposite with 0.5 wt% CNT was out of the measurement range of the multimeter, hence the EC was considered zero. The EC starts to increase substantially upon the addition of 1.5 wt% CNTs to reach 1.6 $10^{-4}$ S/m for DWCNT

and 6.1 $10^{-4}$ S/m for MWCNT-short. Furthermore, an abrupt increase in EC was observed when increasing the MWCNT concentrations to 4 wt%, reaching values of 5 $10^{-3}$ S/m and 4 $10^{-2}$ S/m forDWCNT and MWCNT-short, respectively. The difference in EC values about an order of magnitude between the two types of CNT is once again mainly due to the dispersion state which rules the percolation of the conductive particles and hence favors the EC for the better-dispersed nanotubes which are in the present case the short CNTs (MCNT-4). By examining the cross-section SEM images in Fig. 7, one can clearly notice the presence of DWCNT agglomerates (highlighted with red circles) suggesting a poor dispersion of the CNTs. On the other hand, the short CNTs display a good dispersion in the PFA, with no visible agglomerates. The overall EC is higher than that reported by Lanticse et al. which was about $10^{-5}$ S/m for 5 wt% of MWCNT in the PFA matrix [25]. It is also worth mentioning that the measured electrical conductivity is underestimated since it does not consider the contact resistance between the probe placed on the filament surface and the material.

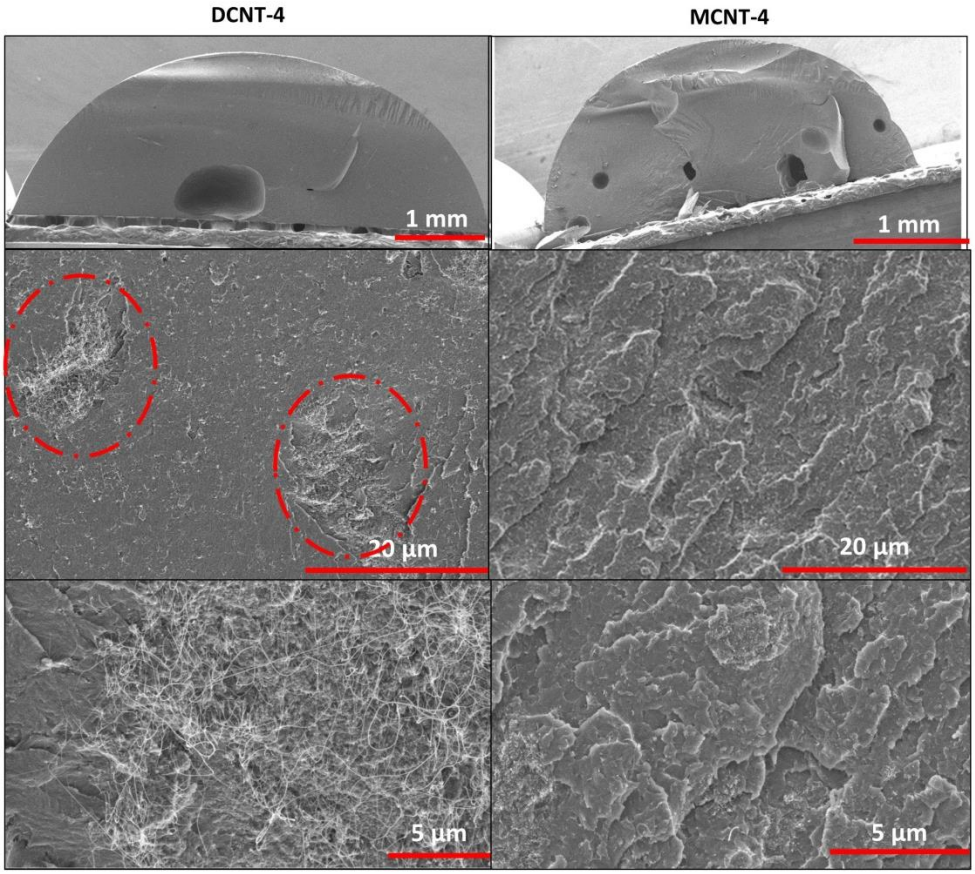


*Fig. 7. SEM images at different magnitudes of the cross-section of a cured nanocomposite filament containing 4 wt% of MWCNT-short (right) and DWCNT (left).*

The electrical conductivity of the composites containing an equal mass fraction of CNT (4 wt%) and 15 wt% and 20 wt% of cellulose powder was measured and is shown in Fig. 8. After the incorporation of 15 wt% of cellulose, the electrical conductivity increased by one order of magnitude for both CNT types with a further increase takes place when adding 5 wt% more cellulose, thus reaching 4.5 $10^{-1}$ S/m. This phenomenon is explained by a decrease in the percolation threshold of the CNT after the incorporation of the inert filler. The filler occupies a certain volume in the composite which makes the space occupied by the PFA/CNT dispersion less important. This redistribution of the conductive particles increases the contact probability among the nanotubes, which therefore decreases the percolation

threshold with the same overall CNT concentration in the composite and thus increases the electrical conductivity. The CNT arrangement in the composite with and without cellulose powder is illustrated in Fig. 9 for a better understanding. This phenomenon is also explained by Bao et al., who introduced the concept of the effective concentration of CNT as the ratio between the CNT volume and the sum of the CNT and the polymer volumes [32]. The effective concentration in our case was calculated on the weight base according to equation (2) and found to be respectively 0.048 and 0.050 when adding 15 and 20 wt% cellulose against 0.04 without any inert particles, which explains the increase in EC.

$$\mathrm{CNT_{eff}} = \frac{\mathrm{W_{CNT}}}{\mathrm{W_{(CNT+PFA)}}} \qquad (2)$$

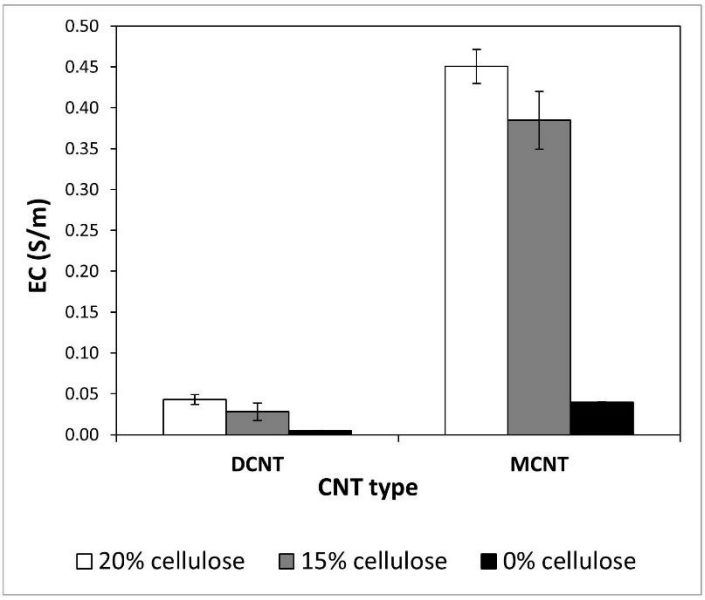


*Fig. 8. Electrical conductivity of composite containing 4 wt% of CNT with different cellulose contents.*

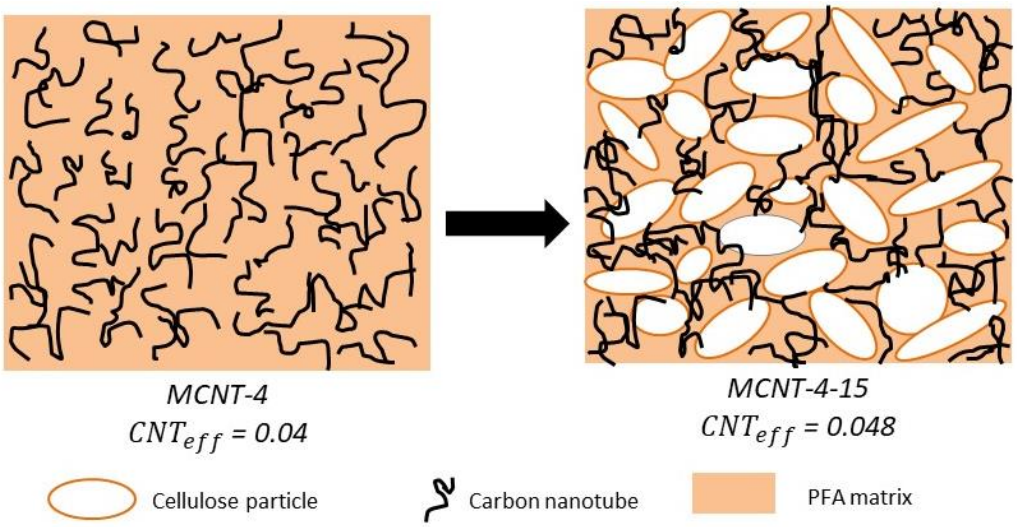


*Fig. 9. Illustration of the influence of cellulose powder on the arrangement of CNT in the composite: (left) PFA/CNT composite without inert particles, (right) PFA/CNT/cellulose powder composite.*

SEM cross-section images of a fractured MCNT-4-15 filament are shown in Fig. 10. First, one can notice a perfect circular shape of the filament in Fig. 10-A, suggesting a higher stiffness and better resistance to the gravitational forces compared with the cellulose-free nanocomposites shown in Fig. 7, where the structure collapsed. These observations are in agreement with the rheological data and suggest a high potential for 3D printing by DIW. In Fig. 10-B, a good dispersion of cellulose particles in the nanocomposite can be observed. Moreover, in Fig. 10-C one can see how the CNT particles (visible in white on the zoomed SEM image) are dispersed in the polymer and arranged in the space between the cellulose particles (outlines highlighted with red lines) confirming the concept of CNT effective concentration discussed previously and illustrated in Fig. 9. These observations corroborate the latter conclusions about the effect of the addition of cellulose particles on the percolation of CNT.

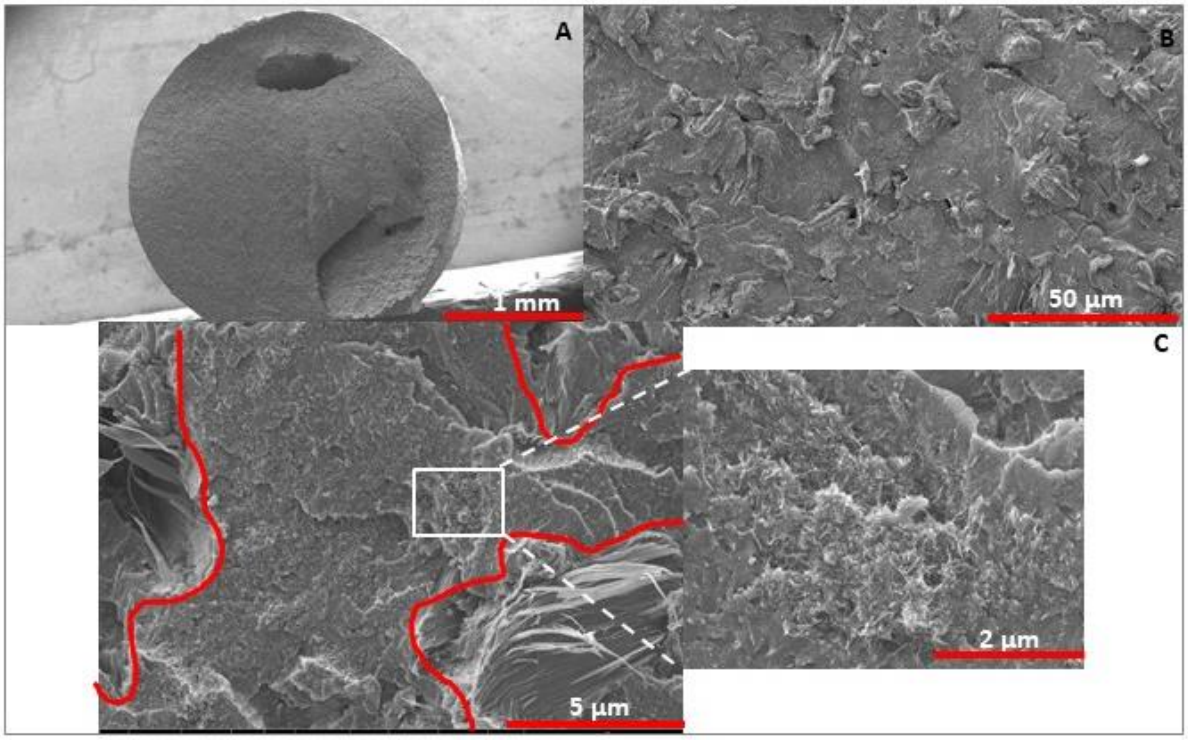


*Fig. 10. SEM images of the cross-section of a cured extruded filament of a nanocomposite containing 4 wt% of MWCNT-short and 15 wt% of cellulose powder at three different magnifications.*

According to these results, we can conclude that the addition of at least 1.5 wt% of CNT in the PFA matrix is needed to effectively increase the electrical conductivity above 1 mS/m and the addition of cellulose powder enhances the printability potential by enhancing the rheological behavior of the formulation. Moreover, the cellulose particles increased the electrical conductivity by one order of magnitude at constant CNT concentration with respect to the cellulose-free nanocomposite.

In light of these findings, the formulation MCNT-15-4 was selected to be the most relevant to our application as, on the one hand, its rheological properties fulfill 3D printing by extrusion's requirements, and, on the other hand, it exhibits good electrical conductivity values. The addition of 20 wt% cellulose was found to deteriorate the mechanical properties

of the extruded filament which was too fragile. Accordingly, 3D printing tests were conducted using a 0.72 mm nozzle and a printing speed of 900 mm/min. As one can see in Fig. 11, a 4 mm high 3D electrode form with 2 mm large spindles was printed with 0.45 mm layer height at 100% infill. The microscope images (Fig. 11) reveal nicely packed layers despite the slight distortion of the tip of the spindles caused by the stickiness of the paste against the nozzles during trajectory inversion. Moreover, a spanned structure at 40% infill and composed of 4 layers, and surrounded by 1 shell, was successfully printed with well-supported filaments. The 3D-printed objects are electrically conductive as illustrated in Fig. 11.


*Fig. 11. Photographs of 3D-Printed objects (left) with microscope zoom (middle) and lighted led lamp using the conductive objects as a link in a simple electrical circuit (right). With connections shown in the images above, the comb-shaped and the cylindrical mesh objects had an electric resistance of 11.7 and 28.7 kΩ, respectively.*

### 3.2 Towards a better electrical conductivity through pyrolysis

Filaments of composite MCNT-4-15 and the CNT-free composite containing 27% cellulose (PFA-Cell25-B) were pyrolyzed and their electrical conductivity was measured (Fig. 12). As expected, the electrical conductivity increased by 5 orders of magnitude from 4 $10^{-2}$ to 4.7 $10^{3}$ S/m for the composite containing CNTs and 2 $10^{3}$ S/m for the composite without CNTs. These EC values surpass the value reported by Hawes *et al.* of laser-induced carbonization of PFA polymer doped with graphene oxide, which was in the range of 9 $10^{2}$ S/m [33]. The increase in EC conductivity when adding CNT can be explained by the higher conductivity of the percolated CNT (> $10^{4}$ S/m) compared with that of the glassy carbon formed after PFA and cellulose pyrolysis.

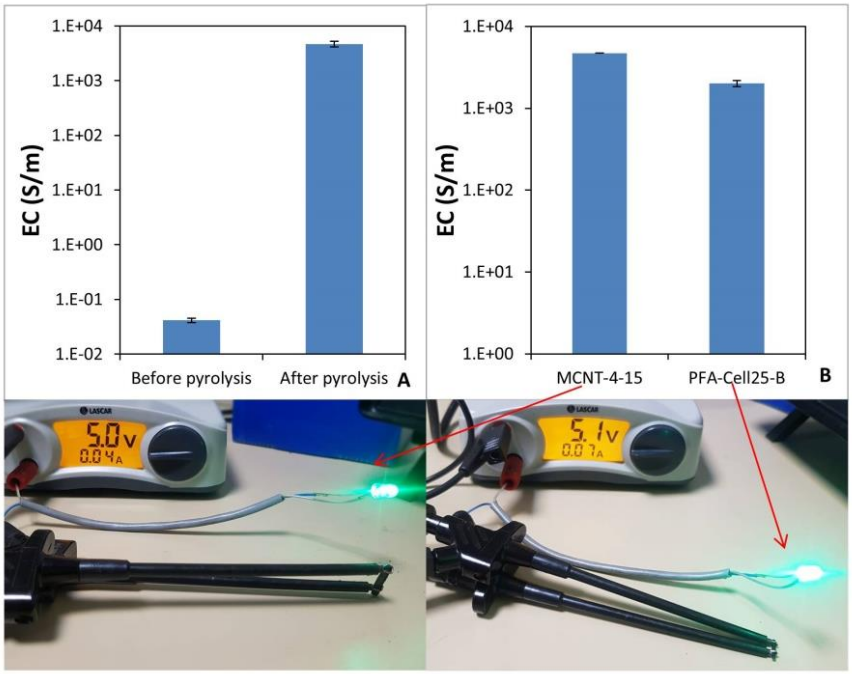


*Fig. 12. (A) Electrical conductivity of the composite MCNT-4-15 before and after pyrolysis and (B) after pyrolysis of composite with and without added CNT.*

From a morphological point of view, one can see on the SEM cross-section images of fractured filaments in Fig. 13 that the PFA-Cell25-B composite conserved its main circular form and that the rough cross-section transformed into a smooth glass-like material after pyrolysis. Many macroscopic pores can also be observed before and after pyrolysis, which was most likely caused by the evaporation of volatiles during the curing step, as we can see on the filament image before pyrolysis [34]. In addition to the macropores, the formation of open pores was suspected to facilitate the transport of volatiles and tar products formed during the pyrolysis of PFA [35,36]. This hypothesis was confirmed in another work to show the formation of meso and micropores when heating below 400°C and a complete collapse of the mesoporous structure and the exclusive residue of micropores with a size of 4–5 Å [37]. In the case of the present work, the remaining micropores after the heat treatment at 950°C were out of the limit of the SEM resolution.

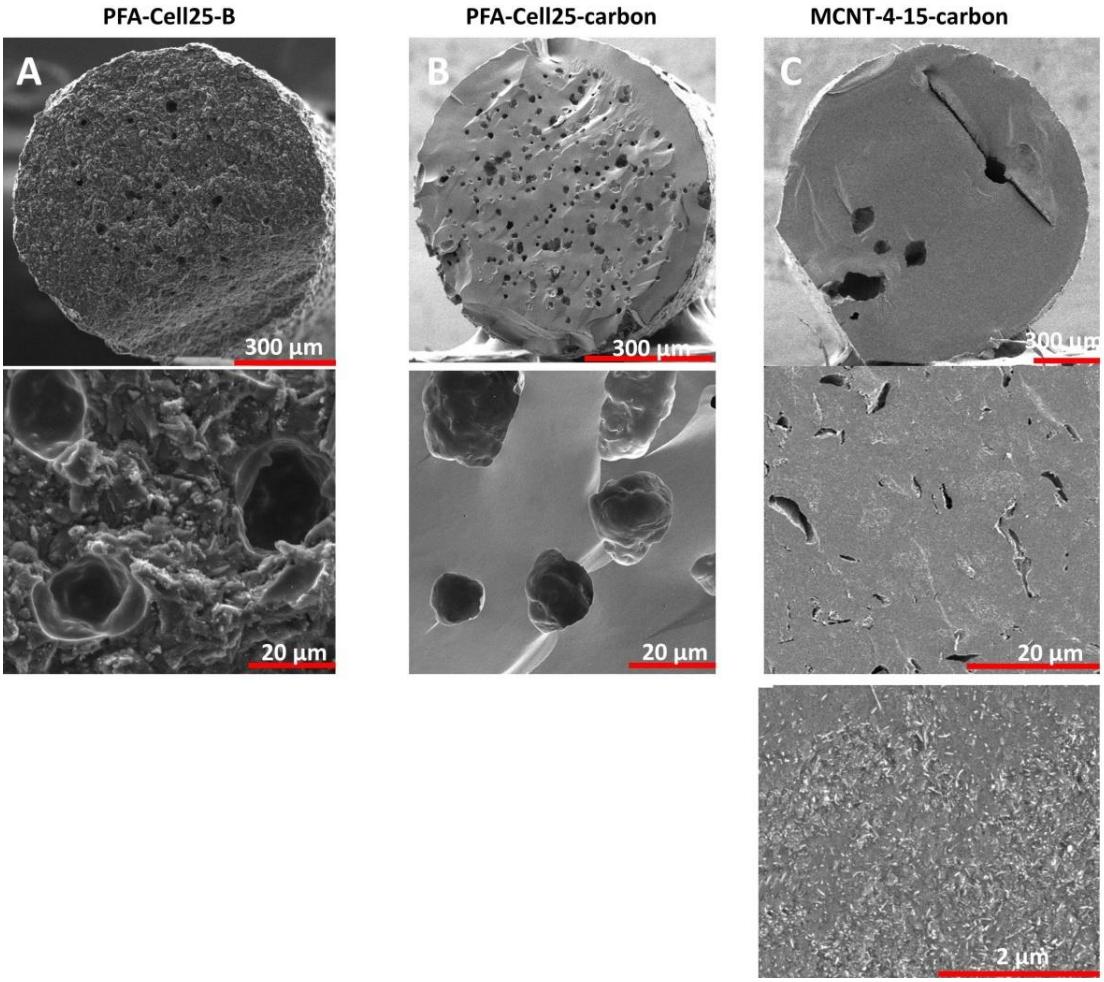


*Fig. 13. SEM images of the cross-section of (A) a cured extruded filament of PFA-Cell25-B composite, (B) a carbonized filament of PFA-Cell25-B composite, and (C) a carbonized filament of nanocomposite (MCNT-4-15) containing 4 wt% of MWCNT-short and 15 wt% of cellulose powder at three different magnifications.*

For large samples, pure glassy carbon is obtained only using temperatures as high as 2000°C or more to ensure effective annealing of volatiles from the core of the sample [38]. However, it was demonstrated that for samples with dimensions <3 mm, which is the case of the used filament in this work, a temperature as low as 900°C was enough to yield a glassy carbon with some oxygen impurities [39]. The lower electric conductivity obtained in the present study (2 $10^3$ S/m), with respect to the electrical conductivity of pure glassy carbon,

might be due to the not compensated contact resistance when the EC conductivity was measured.

## 4 Conclusions

3D printing of electrically conductive inks gained the interest of many researchers lately and more recently the use of the DIW was shown to be a beneficial and low-cost technique to manufacture functional and customized objects. In this work, an ink formulation with a high potential for additive manufacturing by DIW for the manufacturing of bio-based semi-conductive composite was successfully developed. The formulation containing 4 wt% of MWCNTs with a low aspect ratio and 15 wt% cellulose exhibited the best rheological performances, and electrical conductivity values reaching at least 3.85 $10^{-1}$ S/m. CNTs with low aspect ratio were selected to be used in the developed formulation because of their better dispersibility, hence a better electrical conductivity despite the usual better electrical conductivity of a well-dispersed long CNTs network.

Furthermore, the carbonization of the pristine electrically insulating biocomposite containing 27 wt% cellulose, yielded an increase in its electrical conductivity, to reach 2 $10^{3}$ S/m. Moreover, the electrical conductivity doubled when carbonizing the biocomposite containing 4 wt% of carbon nanotube, to reach 4.7 $10^{3}$ S/m. These different printable biocomposites with tunable electrical conductivity, can allow the direct fabrication of conductive structures with tailored 3D objects and enable the integration of electronic functionalities into complex 3D structures.

**Declaration of competing interest**

The authors declare that they have no known competing financial interests or personal relationships that could have appeared to influence the work reported in this paper.

**Acknowledgments**

This work was supported by the Région Rhône-Alpes with Pack Ambition Recherche 3DPapEl 2017-2021 grant and Labcom IDEX Thermobiocomp3D 2019-2022 grant. The LGP2 laboratory is part of the LabEx Tec 21 (Investissements d'Avenir: grant agreement no. ANR-11-LABX-0030) and the PolyNat Carnot Institute (Investissements d'Avenir: grant agreement no. ANR-16-CARN-0025-01). This research was possible owing to the facilities of the TekLiCell platform funded by the Région Rhône-Alpes (ERDF: European Regional Development Fund).

The authors would like to acknowledge Transfurans Chemicals for generously providing the furan resin and the curing agent and Rossow for kindly providing the cellulose powder used in this work.

**References**

[1] R.D. Farahani, M. Dubé, D. Therriault, Three-Dimensional Printing of Multifunctional Nanocomposites: Manufacturing Techniques and Applications, Advanced Materials. 28 (2016) 5794–5821. https://doi.org/10.1002/adma.201506215.

[2] S.L. Marasso, M. Cocuzza, V. Bertana, F. Perrucci, A. Tommasi, S. Ferrero, L. Scaltrito, C.F. Pirri, PLA conductive filament for 3D printed smart sensing applications, Rapid Prototyping Journal. 24 (2018) 739–743. https://doi.org/10.1108/RPJ-09-2016-0150.

[3] S. T, S. P, P. C, Application of 3D printed PLA-carbon black conductive polymer composite in solvent sensing, Mater. Res. Express. 6 (2019) 115349. https://doi.org/10.1088/2053-1591/ab5040.

[4] B. Guo, X. Ji, W. Wang, X. Chen, P. Wang, L. Wang, J. Bai, Highly flexible, thermally stable, and static dissipative nanocomposite with reduced functionalized graphene

oxide processed through 3D printing, Composites Part B: Engineering. 208 (2021) 108598. https://doi.org/10.1016/j.compositesb.2020.108598.

[5] S.S. Athukorala, T.S. Tran, R. Balu, V.K. Truong, J. Chapman, N.K. Dutta, N. Roy Choudhury, 3D Printable Electrically Conductive Hydrogel Scaffolds for Biomedical Applications: A Review, Polymers. 13 (2021) 474. https://doi.org/10.3390/polym13030474.

[6] B.G. Compton, N.S. Hmeidat, R.C. Pack, M.F. Heres, J.R. Sangoro, Electrical and Mechanical Properties of 3D-Printed Graphene-Reinforced Epoxy, JOM. 70 (2018) 292–297. https://doi.org/10.1007/s11837-017-2707-x.

[7] K.M.O. Håkansson, I.C. Henriksson, C. de la P. Vázquez, V. Kuzmenko, K. Markstedt, P. Enoksson, P. Gatenholm, Solidification of 3D Printed Nanofibril Hydrogels into Functional 3D Cellulose Structures, Advanced Materials Technologies. 1 (2016) 1600096. https://doi.org/10.1002/admt.201600096.

[8] K. G. Nair, D. Jayaseelan, P. Biji, Direct-writing of circuit interconnects on cellulose paper using ultra-long, silver nanowires based conducting ink, RSC Advances. 5 (2015) 76092–76100. https://doi.org/10.1039/C5RA10837C.

[9] G. Postiglione, G. Natale, G. Griffini, M. Levi, S. Turri, Conductive 3D microstructures by direct 3D printing of polymer/carbon nanotube nanocomposites via liquid deposition modeling, Composites Part A: Applied Science and Manufacturing. 76 (2015) 110–114. https://doi.org/10.1016/j.compositesa.2015.05.014.

[10] S.R. Shin, R. Farzad, A. Tamayol, V. Manoharan, P. Mostafalu, Y.S. Zhang, M. Akbari, S.M. Jung, D. Kim, M. Comotto, N. Annabi, F.E. Al-Hazmi, M.R. Dokmeci, A. Khademhosseini, A Bioactive Carbon Nanotube-Based Ink for Printing 2D and 3D

Flexible Electronics, Advanced Materials. 28 (2016) 3280–3289. https://doi.org/10.1002/adma.201506420.

[11] M. Vatani, E.D. Engeberg, J.-W. Choi, Force and slip detection with direct-write compliant tactile sensors using multi-walled carbon nanotube/polymer composites, Sensors and Actuators A: Physical. 195 (2013) 90–97. https://doi.org/10.1016/j.sna.2013.03.019.

[12] M. Wei, F. Zhang, W. Wang, P. Alexandridis, C. Zhou, G. Wu, 3D direct writing fabrication of electrodes for electrochemical storage devices, Journal of Power Sources. 354 (2017) 134–147. https://doi.org/10.1016/j.jpowsour.2017.04.042.

[13] S. Nesaei, M. Rock, Y. Wang, M.R. Kessler, A. Gozen, Additive Manufacturing With Conductive, Viscoelastic Polymer Composites: Direct-Ink-Writing of Electrolytic and Anodic Poly(Ethylene Oxide) Composites, Journal of Manufacturing Science and Engineering. 139 (2017). https://doi.org/10.1115/1.4037238.

[14] C. Duty, C. Ajinjeru, V. Kishore, B. Compton, N. Hmeidat, X. Chen, P. Liu, A.A. Hassen, J. Lindahl, V. Kunc, What makes a material printable? A viscoelastic model for extrusion-based 3D printing of polymers, Journal of Manufacturing Processes. 35 (2018) 526–537. https://doi.org/10.1016/j.jmapro.2018.08.008.

[15] M. Sangermano, A. Vitale, N. Razza, A. Favetto, M. Paleari, P. Ariano, Multilayer UV-cured organic capacitors, Polymer. 56 (2015) 131–134. https://doi.org/10.1016/j.polymer.2014.11.021.

[16] A.E. Eken, E.J. Tozzi, D.J. Klingenberg, W. Bauhofer, Combined effects of nanotube aspect ratio and shear rate on the carbon nanotube/polymer composites, Polymer. 53 (2012) 4493–4500. https://doi.org/10.1016/j.polymer.2012.07.045.

[17] J. Li, P.C. Ma, W.S. Chow, C.K. To, B.Z. Tang, J.-K. Kim, Correlations between Percolation Threshold, Dispersion State, and Aspect Ratio of Carbon Nanotubes, Advanced Functional Materials. 17 (2007) 3207–3215. https://doi.org/10.1002/adfm.200700065.

[18] F. Lionetto, A. Greco, D. Pisignano, A. Maffezzoli, Carbon nanotube alignment in a thermosetting resin, AIP Conference Proceedings. 1599 (2014) 190–193. https://doi.org/10.1063/1.4876810.

[19] C. Schilde, M. Schlömann, A. Overbeck, S. Linke, A. Kwade, Thermal, mechanical and electrical properties of highly loaded CNT-epoxy composites – A model for the electric conductivity, Composites Science and Technology. 117 (2015) 183–190. https://doi.org/10.1016/j.compscitech.2015.06.013.

[20] A.T. Seyhan, F.H. Gojny, M. Tanoğlu, K. Schulte, Rheological and dynamic-mechanical behavior of carbon nanotube/vinyl ester–polyester suspensions and their nanocomposites, European Polymer Journal. 43 (2007) 2836–2847. https://doi.org/10.1016/j.eurpolymj.2007.04.022.

[21] M.P. Manoharan, H. Lee, R. Rajagopalan, H.C. Foley, M.A. Haque, Elastic Properties of 4–6 nm-thick Glassy Carbon Thin Films, Nanoscale Res Lett. 5 (2010) 14–19. https://doi.org/10.1007/s11671-009-9435-2.

[22] R. Rajagopalan, A. Ponnaiyan, P.J. Mankidy, A.W. Brooks, B. Yi, H.C. Foley, Molecular sieving platinum nanoparticle catalysts kinetically frozen in nanoporous carbon, Chem. Commun. (2004) 2498–2499. https://doi.org/10.1039/B407854C.

[23] S. Sharma, Glassy Carbon: A Promising Material for Micro- and Nanomanufacturing, Materials. 11 (2018) 1857. https://doi.org/10.3390/ma11101857.

[24] Z. Li, H.R. Kandel, E. Dervishi, V. Saini, Y. Xu, A.R. Biris, D. Lupu, G.J. Salamo, A.S. Biris, Comparative Study on Different Carbon Nanotube Materials in Terms of Transparent

Conductive Coatings, Langmuir. 24 (2008) 2655–2662. https://doi.org/10.1021/la701880h.

[25] L.J. Lanticse, Y. Tanabe, K. Matsui, Y. Kaburagi, K. Suda, M. Hoteida, M. Endo, E. Yasuda, Shear-induced preferential alignment of carbon nanotubes resulted in anisotropic electrical conductivity of polymer composites, Carbon. 44 (2006) 3078–3086. https://doi.org/10.1016/j.carbon.2006.05.008.

[26] N. Guigo, A. Mija, R. Zavaglia, L. Vincent, N. Sbirrazzuoli, New insights on the thermal degradation pathways of neat poly(furfuryl alcohol) and poly(furfuryl alcohol)/SiO2 hybrid materials, Polymer Degradation and Stability. 94 (2009) 908–913. https://doi.org/10.1016/j.polymdegradstab.2009.03.008.

[27] Z. Wang, Z. Lu, Y. Huang, R. Xue, X. Huang, L. Chen, Characterizations of crystalline structure and electrical properties of pyrolyzed polyfurfuryl alcohol, Journal of Applied Physics. 82 (1997) 5705–5710. https://doi.org/10.1063/1.366434.

[28] P.-C. Ma, N.A. Siddiqui, G. Marom, J.-K. Kim, Dispersion and functionalization of carbon nanotubes for polymer-based nanocomposites: A review, Composites Part A: Applied Science and Manufacturing. 41 (2010) 1345–1367. https://doi.org/10.1016/j.compositesa.2010.07.003.

[29] Y.Y. Huang, E.M. Terentjev, Dispersion and rheology of carbon nanotubes in polymers, Int J Mater Form. 1 (2008) 63–74. https://doi.org/10.1007/s12289-008-0376-6.

[30] O. Valentino, M. Sarno, N.G. Rainone, M.R. Nobile, P. Ciambelli, H.C. Neitzert, G.P. Simon, Influence of the polymer structure and nanotube concentration on the conductivity and rheological properties of polyethylene/CNT composites, Physica E: Low-Dimensional Systems and Nanostructures. 40 (2008) 2440–2445. https://doi.org/10.1016/j.physe.2008.02.001.

[31] C. McClory, T. McNally, M. Baxendale, P. Pötschke, W. Blau, M. Ruether, Electrical and rheological percolation of PMMA/MWCNT nanocomposites as a function of CNT geometry and functionality, European Polymer Journal. 46 (2010) 854–868. https://doi.org/10.1016/j.eurpolymj.2010.02.009.

[32] H.-D. Bao, Z.-X. Guo, J. Yu, Effect of electrically inert particulate filler on electrical resistivity of polymer/multi-walled carbon nanotube composites, Polymer. 49 (2008) 3826–3831. https://doi.org/10.1016/j.polymer.2008.06.024.

[33] G.F. Hawes, D. Yilman, B.S. Noremberg, M.A. Pope, Supercapacitors Fabricated via Laser-Induced Carbonization of Biomass-Derived Poly(furfuryl alcohol)/Graphene Oxide Composites, ACS Applied Nano Materials. 2 (2019) 6312–6324. https://doi.org/10.1021/acsanm.9b01284.

[34] S.S. Oishi, M.C. Rezende, F.D. Origo, A.J. Damião, E.C. Botelho, Viscosity, pH, and moisture effect in the porosity of poly(furfuryl alcohol), Journal of Applied Polymer Science. 128 (2013) 1680–1686. https://doi.org/10.1002/app.38332.

[35] E. Fitzer, W. Schaefer, S. Yamada, The formation of glasslike carbon by pyrolysis of polyfurfuryl alcohol and phenolic resin, Carbon. 7 (1969) 643–648. https://doi.org/10.1016/0008-6223(69)90518-1.

[36] E. Fitzer, W. Schäfer, The effect of crosslinking on the formation of glasslike carbons from thermosetting resins, Carbon. 8 (1970) 353–364. https://doi.org/10.1016/0008-6223(70)90075-8.

[37] C.L. Burket, R. Rajagopalan, A.P. Marencic, K. Dronvajjala, H.C. Foley, Genesis of porosity in polyfurfuryl alcohol derived nanoporous carbon, Carbon. 44 (2006) 2957–2963. https://doi.org/10.1016/j.carbon.2006.05.029.

[38] R.N. Hancox, G.D. Lamb, R.S. Lehrle, Sample size dependence in pyrolysis: An embarrassment, or a utility?, Journal of Analytical and Applied Pyrolysis. 19 (1991) 333–347. https://doi.org/10.1016/0165-2370(91)80054-C.

[39] H. Maleki, L.R. Holland, G.M. Jenkins, R.L. Zimmerman, Determining the shortest production time for glassy carbon ware, Carbon. 35 (1997) 227–234. https://doi.org/10.1016/S0008-6223(96)00144-3.

**Figure captions**



**Table captions**